ACS APPLIED MATERIALS & INTERFACES

Research Article

www.acsami.org

Single Walled Carbon Nanotube–Metal Oxide Nanocomposites for Reversible and Reproducible Storage of Hydrogen

D. Silambarasan,[†] V. J. Surya,[‡] V. Vasu,*[,†] and K. Iyakutti[§]

[†]School of Physics, Madurai Kamaraj University, Madurai 625021, Tamil Nadu, India

[‡]New Industry Creation Hatchery Center, Tohoku University, Sendai 980-8579, Japan

[§]Department of Physics & Nanotechnology, SRM University, Kattankulathur 603203, Tamil Nadu, India

Supporting Information

ABSTRACT: Composite material consisting of single walled carbon nanotubes (SWCNTs) and metal oxide nanoparticles has been prepared and their hydrogen storage performance is evaluated. Metal oxides such as tin oxide (SnO_2), tungsten trioxide (WO_3), and titanium dioxide (TiO_2) are chosen as the composite constituents. The composites have been prepared by means of ultrasonication. Then, the composite samples are deposited on alumina substrates and at 100 °C in a Sieverts-like hydrogenation setup. Characterization techniques such as transmission electron microscopy (TEM), Raman spectroscopy, scanning electron microscopy (SEM), powder X-ray diffraction (XRD), Fourier transform infrared (FTIR) spectroscopy, energy dispersive spectroscopy (EDS), CHN elemental analysis, and thermogravimetric (TG) measurements are used to analyze the samples at various stages of experiments. Hydrogen storage capacity of the composites namely, SWCNT–SnO_2, SWCNT–WO_3, and SWCNT–TiO_2 are found to be 1.1, 0.9, and 1.3 wt %, respectively. Hydrogenated composite samples are stable at room temperature and desorption of hydrogen is found to be 100% reversible. Desorption temperature ranges and binding energy ranges of hydrogen have been measured from the desorption studies. The hydrogenation, dehydrogenation temperature, and binding energy of hydrogen fall in the recommended range of a suitable hydrogen storage medium applicable for fuel cell applications. Reproducibility and deterioration level of the composite samples have also been examined.

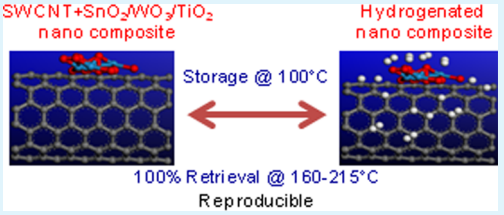

KEYWORDS: *single walled carbon nanotube–metal oxide composite, hydrogen, storage capacity, desorption temperature, reproducibility, deterioration*

INTRODUCTION

Currently, hydrogen is emerging as a clean fuel for transportation applications. The main issues related to safety and leakage while its storage in the form of gas and liquid have led to the storage of hydrogen in its solid state form in materials particularly, nanomaterials. In the group of nanomaterials, carbon nanotubes (CNTs) are emerging as one of the possible hydrogen storage media.[1−4] Primary investigations of hydrogen storage on bare CNTs indicate that CNTs are not suitable material for hydrogen storage.[5−7] But, further investigations based on the modification of CNTs via functionalization and addition of metal ions/atoms show enhanced hydrogen storage performance over bare CNTs.[8−15] Recent reports show that the nanostructured composite materials comprising CNTs and metal oxides are efficient hydrogen storage materials.[16−19] The composite material made up of CNTs and metal oxides such as tin dioxide (SnO_2), tungsten trioxide (WO_3), and titanium dioxide (TiO_2) have been extensively investigated for gas sensor applications,[20−23] and interestingly, the interactions between hydrogen and these metal oxides have also been reported.[24−27] A single walled carbon nanotube (SWCNT) SnO_2 composite thin film prepared by electron beam evaporation technique show a storage capacity of 2.4 wt %, while SnO_2 alone shows a storage capacity of 0.6 wt %. The desorption temperature of hydrogen from the SWCNT–SnO_2 composite is found to be in the range of 200–350 °C.[16] A composite material containing SWCNTs and WO_3 prepared by an electron beam evaporation technique exhibits a hydrogen storage capacity of 2.7 wt %, in which WO_3 shows a storage capacity of 0.5 wt % single handedly, and desorption of hydrogen from the composite occurred in the temperature range of 175–305 °C.[17] Mishra et al.[18] examined the hydrogen storage capacity of CNT–TiO_2 nanotubular hybrid material at 77 and 298 K. The uptake of hydrogen at 77 and 298 K are found to be 2.5 wt % at 25 bar and 1.04 wt % at 22 bar, respectively. In this, TiO_2 nanotubes alone stored 2 wt % of hydrogen at 77 K and 0.9 wt % at 298 K and CNTs stored 0.4 wt % under identical conditions at 77 K. The CNTs impregnated with TiO_2-nanorods and nanotubes show a hydrogen storage capacity of 0.35 and 0.4 wt %, respectively at 298 K and 18 atm, which is nearly five times higher uptake than pristine CNTs.[19] These reports exploring the synergistic

Received: August 29, 2013
Accepted: October 11, 2013
Published: October 11, 2013

effects of CNTs and metal oxide nanostructures, which lead to a better storage and retrieval of hydrogen compared to the components alone.

Hence, the present work is devoted to study the hydrogenation and dehydrogenation properties of composites made by SWCNTs and metal oxide nanoparticles such as SnO_2, WO_3, and TiO_2. Ultrasonication is one of the facile methods used for the preparation of CNT−metal oxide composite.[19] We have also used the same method to prepare the composites SWCNT−SnO_2, SWCNT−WO_3, and SWCNT−TiO_2. The composites have been prepared by means of ultrasonication in 2-proponal medium. The well-dispersed solution is then deposited on alumina substrates by drop casting approach. Then, the samples are hydrogenated in a Sieverts-like hydrogenation setup.[27] The hydrogenation of CNT−metal oxide composite reported in earlier investigations[18,19] was carried out at very low temperatures and at some pressure conditions. Here, the hydrogenation experiments are conducted above room temperature, i.e. at 100 °C. Hydrogen storage capacity, desorption temperature range, and binding energy range of hydrogen have been measured based on the characterization results. To check the reproducibility and deterioration level of the composite samples, we have repeated the hydrogenation and dehydrogenation experiments and the results are presented.

EXPERIMENTAL SECTION

Materials. SWCNTs with a purity of >98% and metal oxide nanoparticles with 99% minimum assay were purchased from Sigma Aldrich. The other reagents and chemicals used for experiments were purchased from Merck with 99% purity. Alumina substrates of dimension 19 × 19 × 0.65 mm were cleaned with chromic acid, acetone, and distilled water by means of sonication for 30 min (alumina substrates were used as it will not react while heating).

Purification of SWCNTs. Generally, the commercial CNTs contain the major component CNTs along with amorphous carbon structures and metal catalyst impurities in few percentages. Hence, the purification of CNTs is necessary before conducting experiments. The expected amorphous carbon structures present in the purchased SWCNTs was removed by heating them in a tubular furnace at 300 °C for 1 h. After the heat treatment, the SWCNTs were mixed with the solution containing the mixture of nitric acid and sulphuric acid. Further, this solution was ultrasonicated for 8 h and the solution containing dispersed SWCNTs was left overnight. Finally, leaving behind the precipitate of impurities, the upper suspended SWCNT solution was collected. The solution was filtered and washed several times using double distilled water until the pH of the solution reached around 6. In this way, the purchased SWCNTs were purified. These purified SWCNTs were used for experiments.

Composite Preparation. The purified SWCNTs (50 mg) and metal oxide nanoparticles (100 mg) were taken in a ratio of 1:2 by weight and ground well for 30 min. The mixture was then taken with 10 mL of 2-propanol. This solution was then kept in an ultrasonic bath at room temperature for 3 h to allow the components for uniform dispersion. The dispersed solution was then deposited dropwise using a micropipet on alumina substrates that were maintained in air ∼70 °C. The highly volatile 2-proponal got evaporated and left the composite on the substrates. After deposition, the substrates were heated to 200 °C for 1 h to remove the impurities if any.

Hydrogenation. The composite samples were loaded in Sieverts-like hydrogenation setup and hydrogenated as detailed below. The samples were maintained at 100 °C, and the hydrogen was allowed to flow for 20 min at a constant flow rate of ∼0.2 L/min, and then the samples were left in the chamber to attain room temperature. After that, the hydrogen content present in the samples was estimated. The hydrogen storage capacities of the samples are presented in Table 1.

Table 1. Summary of Hydrogen Storage Capacity of the Samples

samples	temperature (°C)	hydrogen content (wt %)
SWCNTs	100	0.05
SWCNT−SnO_2	100	1.1
SWCNT−WO_3	100	0.9
SWCNT−TiO_2	100	1.3

Dehydrogenation. To check the desorption of hydrogen from the hydrogenated composite samples, we have used thermal annealing approach. Thermal annealing is believed to be one of the methods to stimulate dehydrogenation process.[28,29] In this process, the hydrogenated composite samples were annealed at 300 °C for 1 h in a muffle furnace. After annealing, the samples were left in the furnace to reach room temperature and then characterized.

Characterization. The morphology of SWCNTs was imaged by transmission electron microscopy (TEM) using JEOL JEM 2100 model unit with an accelerating voltage of 200 kV. Raman measurements were carried out in Renishaw InVia model spectrometer with the laser excitation of 514 nm. Scanning electron microscopy (SEM) images and energy dispersive X-ray spectrum (EDS) were recorded using JEOL-MODEL 6390 unit with an accelerating voltage of 5 kV. Powder X-ray diffraction (XRD) study was performed on XPERT-PRO diffractometer operating at 40 kV and 30 mA, using Cu Kα radiation. Fourier transform infrared (FTIR) spectra were recorded using FTIR-8400, CE, Shimadzu model spectrometer at room temperature in the range of 4500−400 cm^{-1} with a resolution of 1 cm^{-1}. CHN elemental analysis was carried out using Elementar Vario EL III model analyzer. The thermogravimetric (TG) measurements were carried out using Perkin-Elmer-Diamond model unit over the temperature range of 30−400 °C at a scanning rate of 10 °C/min.

RESULTS AND DISCUSSION

The TEM image of purified SWCNTs is shown in Figure 1a. The image reveals the well-distributed and separated high

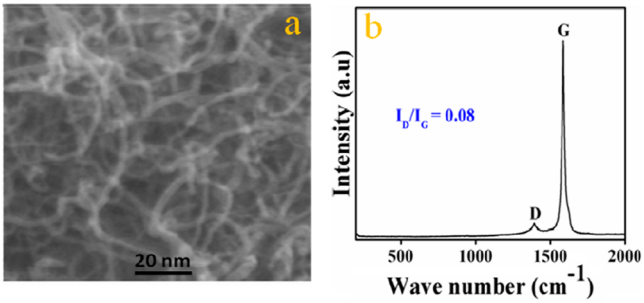

Figure 1. (a) TEM image and (b) Raman spectrum of SWCNTs.

quality SWCNTs with the estimated average diameter in the range of 2−4 nm. Figure 1b shows the Raman spectrum of SWCNTs. In general, the disordered (D) and graphitic (G) bands are the two characteristics bands for CNTs. The D band generally appears in the range 1300−1400 cm^{-1} and is typically assigned to the presence of amorphous/disordered carbon in CNTs. The tangential (G) mode is the strong and most intensive high-energy mode of SWCNTs, which is usually observed in the range 1565−1595 cm^{-1}. The G band arises due to in-plane tangential stretching of C−C bonds in CNTs. In this mode, the displacement of carbon atoms exists in the circumferential direction. As expected, the two bands namely D and G appear in the spectrum in their corresponding range. Generally, in Raman spectrum of SWCNTs the intensity ratio of D to G band is a measure of defects concentration in the

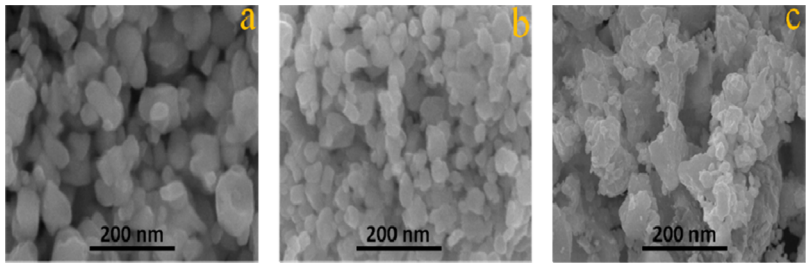

Figure 2. SEM images of (a) SnO_2, (b) WO_3, and (c) TiO_2 nanoparticles.

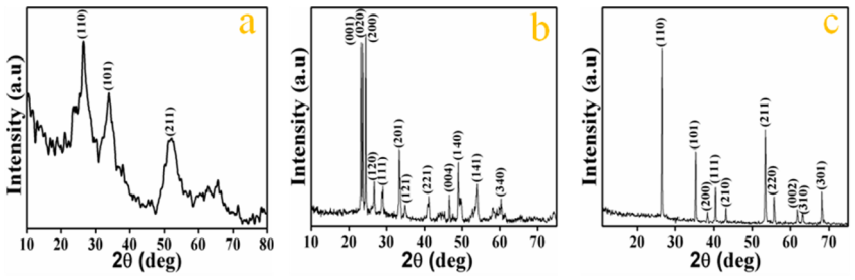

Figure 3. XRD pattern of (a) SnO_2, (b) WO_3, and (c) TiO_2 nanoparticles.

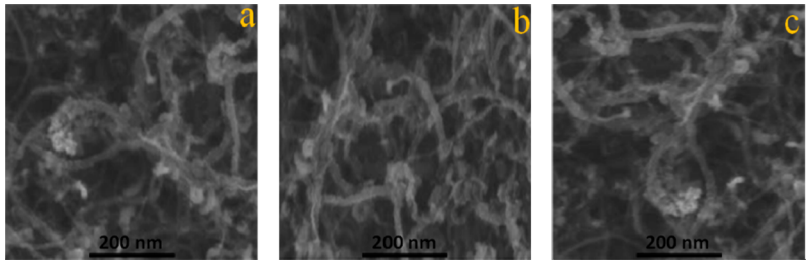

Figure 4. SEM images of (a) SWCNT−SnO_2, (b) SWCNT−WO_3, and (c) SWCNT−TiO_2 composites.

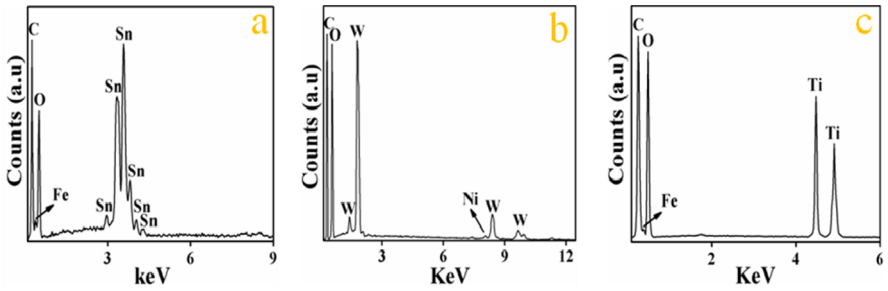

Figure 5. ED spectra of (a) SWCNT−SnO_2, (b) SWCNT−WO_3, and (c) SWCNT−TiO_2 composite.

samples. The D/G intensity ratio is measured to be 0.08 and this lower value indicates the presence of lesser amount of defect/amorphous carbon concentration in SWCNTs.

Figure 2 parts a, b, and c show the SEM images of SnO_2, WO_3, and TiO_2 nanoparticles, respectively. The nanoparticles have an average diameter distribution in the range 10−80, 10−40, and 10−50 nm for SnO_2, WO_3, and TiO_2, respectively. The XRD spectra of SnO_2, WO_3, and TiO_2 nanoparticles are presented in Figure 3 parts a, b, and c, respectively. In Figure 3a, the strong diffraction peaks appearing for (110), (101), and (211) planes indicate the crystalline face of SnO_2 nanoparticles with (110) as preferred orientation. The diffraction peaks in Figure 3b can be well indexed to orthorhombic WO_3. The XRD pattern shown in Figure 3c exhibits strong diffraction peaks at 27.3°, 36.2°, and 54.4°, which indicates the existence of TiO_2 predominantly in rutile phase. All the appeared diffraction peaks are indexed on the basis of polymorphic phases of crystalline TiO_2, and they are in good agreement with standard pattern. The presence of sharp peaks infers the better crystalline nature of nanoparticles.

Figure 4 shows SEM images of (a) SWCNT−SnO_2, (b) SWCNT−WO_3, and (c) SWCNT−TiO_2 composites. The attachment of nanoparticles to the walls of CNT can be clearly seen. Moreover, the diameter of SWCNTs is increased to 20−25 nm due to attachment of nanoparticles to the walls. The ED spectrum of the SWCNT−SnO_2 composite is shown in Figure 5a. The weight percentages of the elements present in the composite are found to be 40.12, 39.37, and 20.51 for carbon, oxygen, and tin, respectively. The ED spectrum of the SWCNT−WO_3 composite is shown in Figure 5b. The weight

percentages of the elements are 39.98, 39.57, and 20.45 for carbon, oxygen, and tungsten, respectively. The presence of elements in the SWCNT−TiO_2 composite was ascertained from ED spectrum shown in Figure 5c. The weight percentages of the elements present in composite are 40.72, 39.10, and 20.18 for carbon, oxygen, and titanium, respectively. In addition to the materials present in the composite, a small amount (<0.05 wt %) of catalyst particles (Fe, Ni) that are used during the synthesis of CNTs is also observed in each of the ED spectra. The absence of any other peak except those due to the components in the composite is the evidence of the quality of composites without any elemental impurities.

The presence of functional groups and the existence of elements in the composites are confirmed by FTIR analysis. Figure 6 shows the FTIR spectra of composite samples namely,

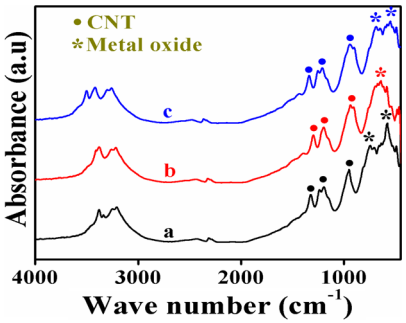

Figure 6. FTIR spectra of (a) SWCNT−SnO_2, (b) SWCNT−WO_3, and (c) SWCNT−TiO_2 composite.

SWCNT−SnO_2 (a), SWCNT−WO_3 (b), and SWCNT−TiO_2 (c), respectively. Absorption peaks around 1340, 1200−1240, and 940 cm^{-1} correspond to C═C in-plane, C═C stretching, and C—C stretching vibrations, respectively in CNTs.[27] This is observed in the spectra of all three samples. The absorption peaks appeared (Figure 6a) around 750 and 580 cm^{-1} correspond to Sn−O and O−Sn−O stretching vibrations. In Figure 6b, the absorption peak appeared around 650 cm^{-1} is due to W−O stretching vibrations in WO_3. The absorption peaks observed around 690 and 550 cm^{-1} in Figure 6c are related to Ti−O vibration in TiO_2 lattice.

Raman spectra of the composite samples SWCNT−SnO_2, SWCNT−WO_3, and SWCNT−TiO_2 are shown in Figures 8a, 9a, and 10a, respectively. The bands corresponding to metal oxide nanoparticles together with the characteristic bands D and G of SWCNTs are observed in these spectra. In these spectra, the intensity of D band has increased and G band has decreased when compared to the Raman spectrum of SWCNTs shown in Figure 1b. The corresponding D/G intensity ratios of the composite samples have also increased, and they are noted in the respective spectra. This again confirms the formation of composite. In addition to that, the Raman modes in Figure 8a around 120 and 630 cm^{-1} correspond to rutile type SnO_2 nanoparticles.[30] In Figure 9a, the Raman modes appearing at 807, 324, 271, and 132 cm^{-1} belong to W−O stretching, O−W−O bending, O−W−O stretching, and W−O−W bending vibrations of WO_3, respectively.[31,32] In Figure 10a, the Raman mode appeared at 629 cm^{-1} belongs to the rutile phase of TiO_2 nanoparticles.[33] The phases of the metal oxide nanoparticles characterized by Raman analysis supports XRD results.

CHN elemental analysis was used to find out the quantity of hydrogen stored in the hydrogenated composite samples. The elemental analysis (CHN/CHNS) method is one of the widely used techniques for the measurement of hydrogen storage as well as the composition of elements such as carbon, hydrogen, nitrogen, and sulfur.[34−36] Before knowing the hydrogen storage capability of composite materials, the hydrogen storage capability of SWCNTs was tested and the hydrogenation results of all the samples are presented in Table 1.

As expected, SWCNTs alone show the least storage capacity under these conditions. This is because naturally, the interaction between hydrogen and bare CNTs is very weak around or above room temperature; one can achieve a stable higher storage capacity at lower temperatures only. On the other hand, the composite samples show a multifold increase in hydrogen storage capacity (when compared to neat SWCNTs), and it is due to the cumulative adsorption of hydrogen by CNTs and metal oxide nanostructure constituents in the composite. Hence, one can confirm that the synergistic effect existing between CNTs and metal oxide nanostructures.[16−19] The FTIR spectra of all the three hydrogenated composite samples are collectively shown in Figure 7. The vibration bands

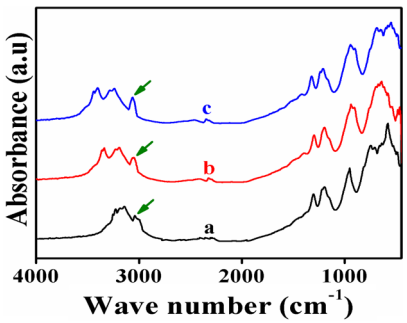

Figure 7. FTIR spectra of hydrogenated (a) SWCNT−SnO_2, (b) SWCNT−WO_3, and (c) SWCNT−TiO_2 composite.

corresponding to the functional groups of CNTs and metal oxide nanoparticles are observed in the same range that are observed in the unhydrogenated composite sample, but in addition to those peaks, a new absorption peak around 3050 cm^{-1} (indicated by arrow) is noted in all the three hydrogenated composite samples. This is attributed to C−H stretching vibration,[29] and it has appeared due to hydrogenation. When we analyze the Raman spectroscopy of the hydrogenated composite samples, significant changes in the spectra are observed. After hydrogenation, the D band intensity has increased and the corresponding G band intensity has decreased. The corresponding D/G ratio has increased due to the increase in defect density in the hydrogenated composite samples.[29,37] The D/G intensity ratio of the hydrogenated composite samples SWCNT−SnO_2, SWCNT−WO_3, and SWCNT−TiO_2 is mentioned in Figures 8b, 9b, and 10b, respectively.

To check the desorption of hydrogen from the hydrogenated samples, we have carried out thermal annealing. The hydrogenated samples were annealed at 300 °C for 1 h, and the entire process was probed by Raman and CHN elemental analyses. It is noted that after annealing, the intensities of D and G bands have decreased and increased respectively, which indicates desorption of hydrogen from the samples. The corresponding CHN elemental analysis also confirms this desorption. The entire hydrogenation and dehydrogenation experiments were repeated for a number of times. The D/G ratio of composite

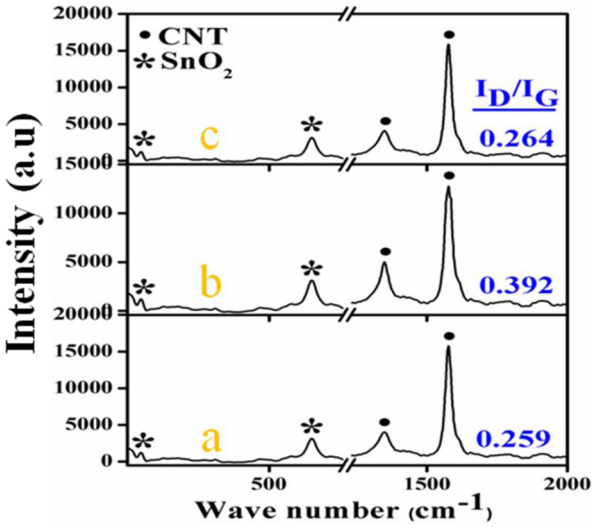

Figure 8. Raman spectra of (a) SWCNT−SnO_2, (b) hydrogenated SWCNT−SnO_2, and (c) dehydrogenated SWCNT−SnO_2 composite.

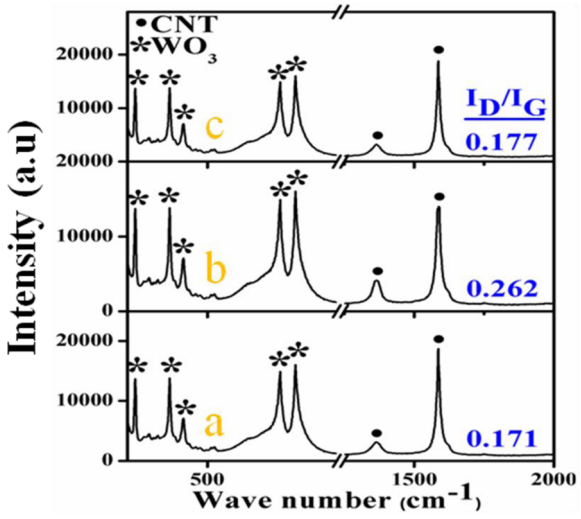

Figure 9. Raman spectra of (a) SWCNT−WO_3, (b) hydrogenated SWCNT−WO_3, and (c) dehydrogenated SWCNT−WO_3 composite.

sample SWCNT−SnO_2 is 0.259 and for the dehydrogenated sample (Figure 8c) the D/G ratio is 0.264. The difference in D/G ratio, from 0.264 to 0.259 is 0.005 (1.9%) after the first cycle. Now, we have hydrogenated this dehydrogenated composite sample under the same conditions. For this second cycle the difference is 0.012 (4.5%). In the third cycle it changes to 6.8%. There is an increase of 2.3−2.6% in the D/G intensity ratio between two successive cycles. If we take the change in D/G intensity ratio of the dehydrogenated SWCNT−SnO_2 composite after each cycle, it is about 2.45%. Similarly, the average change in D/G intensity ratio of the dehydrogenated SWCNT−WO_3 and SWCNT−TiO_2 composite after each cycle, it is about 2.9 and 2.3%, respectively. The entire hydrogenation and dehydrogenation experiment cycles are independent events and this effect is not cumulative. The quality of the composite samples deteriorates due to dehydrogenation is only less than 3%. This indicates that the composite samples are restored to the original level after dehydrogenation. So at the end of any number of cycles, the change in D/G ratio value and the deterioration in the samples

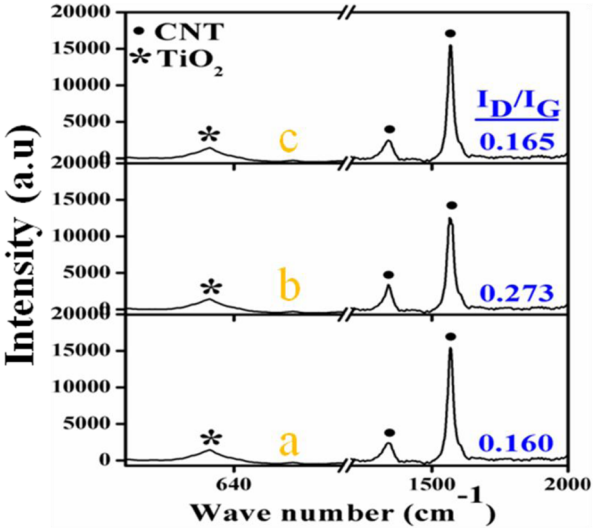

Figure 10. Raman spectra of (a) SWCNT−TiO_2, (b) hydrogenated SWCNT−TiO_2, and (c) dehydrogenated SWCNT−TiO_2 composite.

are less than 3%. This is the limitation in our method. The expected deviation in the hydrogen storage capacity of the composite samples measured by CHN-elemental analysis is within 5% about the mean value. Zhang et al.[37] observed the percentage of change in D/G intensity ratio and it was about 3%. It may be noted that the Raman spectra corresponding to the dehydrogenated and composite samples are similar. This in turn not only confirms desorption of hydrogen from the sample but also shows that the composite samples are recovered after dehydrogenation.

After confirming the desorption of hydrogen from Raman spectroscopy and CHN elemental analysis, the thermogravimetric characterization of hydrogenated composite samples were carried out to find the exact desorption temperature range of hydrogen. The thermogravimetric spectra of hydrogenated composite samples are collectively shown in Figure 11. The

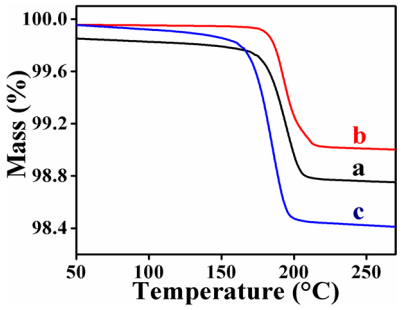

Figure 11. Thermogravimetric spectra of hydrogenated (a) SWCNT−SnO_2, (b) SWCNT−WO_3, and (c) SWCNT−TiO_2 composite.

spectrum corresponding to SWCNT−SnO_2 presented in Figure 11a shows a weight loss of 1.1 wt % in the temperature range, 170−210 °C. This weight loss corresponds to the desorption of hydrogen from the hydrogenated SWCNT−SnO_2 composite sample.

The activation energy of desorption (E_d) can be calculated from the desorption temperature using the following equation[38]

$$\ln\left(\frac{T_m^{\,2}}{\beta}\right) = \frac{E_d}{RT_m}$$

dx.doi.org/10.1021/am403662t | ACS Appl. Mater. Interfaces 2013, 5, 11419−11426

where, T_m is the desorption temperature, β is the heating rate (10 °C/min), and R is the universal gas constant. The binding energy (E_B) of hydrogen is calculated using van't Hoff equation[39] for the desorption temperatures 170 and 210 °C and the values obtained are 0.346 and 0.378 eV, respectively. The corresponding desorption activation energies are 24.1 and 26.9 kJ/mol, respectively. The thermogravimetric spectra of hydrogenated composite samples SWCNT−WO_3 and SWCNT−TiO_2 are shown in Figure 11b and c, respectively. The desorption temperature of hydrogen, activation energy of desorption, and binding energy values are calculated in the same way, and the results are presented in Table 2. The error analysis for activation energy of desorption is carried out and the results are presented in Supporting Information. It is inferred that the thermogravimetric analysis together with CHN elemental analysis provides evidence for the measurement of hydrogen storage in the composite samples.[25,27,29]

Table 2. Desorption Characteristics Parameters

samples	weight loss (wt %)	desorption temperature range (°C)	activation energy of desorption range (kJ/mol)	binding energy range (eV)
SWCNT−SnO_2	1.1	170−210	24.1−26.9	0.346−0.378
SWCNT−WO_3	0.9	175−215	24.4−27.3	0.350−0.381
SWCNT−TiO_2	1.3	160−205	23.3−26.6	0.338−0.373

From the thermogravimetric analysis, it is clear that the amount of hydrogen desorbed is equal to the amount of hydrogen adsorbed by the composite. Hence, all the three hydrogenated composite samples SWCNT−SnO_2, SWCNT−WO_3, and SWCNT−TiO_2 exhibit 100% desorption. Even the hydrogen storage capacities of the composite samples SWCNT−SnO_2 and SWCNT−WO_3 reported here are lower than the storage capacity of the same composite samples reported in refs 16 (2.4 wt.%) and 17 (2.7 wt.%), the desorption temperature range of hydrogen in the present study is lower than the desorption temperature range shown by those composite samples (SWCNT−SnO_2 200−350 °C and SWCNT−WO_3 175−305 °C). On the other hand, it is worthwhile to compare the results of SWCNT−TiO_2 composite with that of Mishra et al.[18] As mentioned earlier, they reported the uptake of hydrogen by CNT−TiO_2 nanotubular hybrid material at 77 and 298 K as 2.5 wt % at 25 bar and 1.04 wt % at 22 bar, respectively. Since our experiments are done at 100 °C and ambient pressure, it is sensible to compare the storage capacity of SWCNT−TiO_2 composite (1.3 wt % at 100 °C and atmospheric pressure) with their latter result (1.04 wt % at 298 K and 22 bar). It can be inferred that our result is slightly higher than the value reported by them. Moreover, our composite sample SWCNT−TiO_2 shows 100% reversibility, while the hydrogen desorption from their composite sample is not 100% reversible and the hydrogenated composite samples reported here are stable at room temperature. Lochan et al.[40] reported that an ideal hydrogen storage medium should store hydrogen in the binding energy range, 0.2−0.4 eV for usage in fuel cell applications. The obtained binding energy of hydrogen in the present case lies in this recommended range. Hence, the present hydrogen storage media may be used for fuel cell applications. This range lies between physisorption and chemisorption limits. Here, the binding energies of hydrogen in all three composite samples fall under this range. Hence, one can emphasize that the adsorbed hydrogen is weakly chemisorbed on the composite network and the entire stored hydrogen molecules are usable. In this binding energy limits, the interaction between the host material and hydrogen molecules is involving primarily due to the combination of electrostatic, inductive, and covalent charge transfer mechanisms.[40] In the present work, the hydrogenation experiments are conducted above the room temperature, i.e. at 100 °C whereas; earlier investigations[18,19] on hydrogenation of CNT−metal oxide composite were carried out at very low temperatures and at certain pressure conditions. Moreover, the deterioration level of the composite samples due to dehydrogenation does not exceed 3% after a number of recyclings of the samples. The entire hydrogenation and dehydrogenation experiment cycles are independent events and this effect is not cumulative. But in the previous cases,[16,17] the composites were prepared and hydrogenated by electron beam evaporation technique. In that case, hydrogenation and dehydrogenation processes are one-time events, i.e., the composite material cannot be recycled. In addition to that, the preparation of the composite samples in the previous cases requires vacuum conditions. But, in the present case the preparation of samples does not require vacuum conditions.

Interestingly, the composite samples show multifold increase in hydrogen storage capacity when compared to neat SWCNTs. This may be due to the general spillover mechanism. This effect is possibly due to the presence of metal or metal oxide nanoparticles networked with high surface area materials like SWCNTs. During hydrogenation, the metal oxide nano particles may dissociate the hydrogen molecule and migrate the hydrogen atoms to the nearest vacant sites on CNTs. More amount of hydrogen can occupy on the adsorption sites offered by CNTs in this way. During the course of desorption, the adsorbed hydrogen atoms were supposed to recombine into molecular hydrogen (this process is known as reverse spillover) and get desorbed from the samples.[41] This kind of adsorption of hydrogen does not require a temperature range more than 250−300 °C to release the stored hydrogen.[42,43] The desorption temperature range of hydrogen observed in this work is in accordance with these reports. Therefore, spillover mechanism may contribute to higher hydrogenation in the composite samples and lower desorption temperature range of hydrogen. The appearance of C−H vibration band in the FTIR spectra of hydrogenated composite samples shown in Figure 7 supports this spillover mechanism. Rather et al.[19] pointed out that the rutile phase of TiO_2 nanoparticles interacts weakly with hydrogen which results in diffusive spillage of hydrogen to CNT binding sites and anatase phase of TiO_2 nanorods strongly bind hydrogen itself and exhibit negligible spillover to CNTs. It seems that the phases of metal oxide nanoparticles play a significant role in the hydrogen storage capacity of the materials. Even though the hydrogen storage capacities of the composite samples reported here are not nearer to the US DOE target for the practical applications; it is important to consider the phases of the metal oxide nanostructures which are efficient in spilling the hydrogen onto CNTs. Further theoretical as well as experimental investigations are obviously needed in order to understand and fine-tune the exact hydrogen adsorption and spillover mechanisms and achieve higher hydrogen storage capacity in these composite materials.

CONCLUSIONS

Hydrogen storage capacity of composite materials consisting of SWCNTs and metal oxide nanoparticles such as SWCNT−SnO_2, SWCNT−WO_3, and SWCNT−TiO_2 have been evaluated. The composites have been prepared by means of ultrasonication in 2-proponal medium. Then, the composite samples are deposited on alumina substrates and hydrogenated at 100 °C in a Sieverts-like hydrogenation setup. Hydrogen storage capacity of the composites namely, SWCNT−SnO_2, SWCNT−WO_3, and SWCNT−TiO_2 are found to be 1.1, 0.9, and 1.3 wt %, respectively. The hydrogenated composite samples are stable at room temperature, and desorption of hydrogen is found to be 100% reversible. Higher hydrogen uptake of the composite materials when compared to neat CNTs is accounted for the spillover mechanism in SWCNT−metal oxide composites. The nature of hydrogen binding in the composite network is found to be weak chemisorption. Desorption temperature range and binding energy of hydrogen have been measured and they are falling in the recommended range of storage medium that to be used in automobile applications. Reproducibility and deterioration level of the composite samples while repeating the hydrogenation and dehydrogenation experiments have also been checked. From the present investigation, it is clear that the composites such as SWCNT−SnO_2, SWCNT−WO_3, and SWCNT−TiO_2 are having the capability of reversible hydrogen storage. They are to be fine-tuned to achieve higher hydrogen storage capacity.

ASSOCIATED CONTENT

Supporting Information

Error analysis for activation energy of desorption. This material is available free of charge via the Internet at http://pubs.acs.org.

AUTHOR INFORMATION

Corresponding Author

*E-mail: vvasumku@gmail.com. Phone: +91 94437 96898.

Notes

The authors declare no competing financial interest.

ACKNOWLEDGMENTS

The authors D.S. and V.V. thank University Grants Commission (UGC), New Delhi, and author K.I. thanks Council of Scientific and Industrial Research (CSIR), New Delhi, for financial support under Emeritus Scientist scheme. The authors thank Dr. T. R. Ravindran, Scientific officer, Indira Gandhi Centre for Atomic Research (IGCAR), Kalpakkam for availing Raman measurements.

REFERENCES

(1) Dillon, A. C.; Jones, K. M.; Bekkendahl, T. A.; Kiang, C. H.; Bethune, D. S.; Heben, M. J. *Nature* **1997**, *386*, 377−379.
(2) Li, J.; Terumi, F.; Hajime, G.; Toshiyuki, O.; Yoshiya, F.; Sidney, Y. *J. Chem. Phys.* **2003**, *119*, 2376−2385.
(3) Han, K. S.; Kim, H. S.; Song, M. S.; Park, M. S.; Han, S. S.; Lee, J. Y.; Kang, J. K.; Kim, Y. K. *Appl. Phys. Lett.* **2005**, *86*, 263105−1−263105−3.
(4) Liu, C.; Chen, Y.; Wu, C.-Z.; Xu, S.-T.; Cheng, H.-M. *Carbon* **2010**, *48*, 452−455.
(5) Rzepka, M.; Lamp, P. *J. Phys. Chem. B* **1998**, *102*, 10894−10898.
(6) Ye, Y.; Ahn, C. C.; Witham, C.; Fultz, B.; Liu, J.; Rinzler, A. G.; Colbert, D.; Smith, K. A.; Smalley, R. E. *Appl. Phys. Lett.* **1999**, *74*, 2307−2309.
(7) Tibbetts, G. G.; Meisner, G. P.; Olk, C. H. *Carbon* **2001**, *39*, 2291−2301.
(8) Kim, H.-S.; Lee, H.; Han, K.-S.; Kim, J.-H.; Song, M.-S.; Park, M.-S.; Lee, J.-Y.; Kang, J.-K. *J. Phys. Chem. B* **2005**, *109*, 8983−8986.
(9) Rather, S.; Zacharia, R.; Hwang, S. W.; Naik, M.; Nahm, K. S. *Chem. Phys. Lett.* **2007**, *441*, 261−267.
(10) Chen, L.; Zhang, Y. M.; Koratkar, N.; Jena, P.; Nayak, S. K. *Phys. Rev. B* **2008**, *77*, 033405−1−033405−8.
(11) Iyakutti, K.; Kawazoe, Y.; Rajarajeswari, M.; Surya, V. J. *Int. J. Hydrogen Energy* **2009**, *34*, 370−375.
(12) Surya, V. J.; Iyakutti, K.; Rajarajeswari, M.; Kawazoe, Y. *Phys. E* **2009**, *41*, 1340−1346.
(13) Gao, L.; Yoo, E.; Nakamura, J.; Zhang, W.; Chua, H. T. *Carbon* **2010**, *48*, 3250−3255.
(14) Reyhani, A.; Mortazavi, S. Z.; Mirershadi, S.; Moshfegh, A. Z.; Parvin, P.; Nozad Golikand, A. *J. Phys. Chem. C* **2011**, *115*, 6994−7001.
(15) Lakshmi, I.; Silambarasan, D.; Surya, V. J.; Rajarajeswari, M.; Iyakutti, K.; Mizuseki, H.; Kawazoe, Y. *Int. J. Nanosci.* **2011**, *10*, 391−396.
(16) Silambarasan, D.; Surya, V. J.; Vasu, V.; Iyakutti, K. *Int. J. Hydrogen Energy* **2013**, *38*, 4011−4016.
(17) Silambarasan, D.; Surya, V. J.; Vasu, V.; Iyakutti, K.; Ravindran, T. R. *Int. J. Hydrogen Energy*, submitted for publication.
(18) Mishra, A.; Banerjee, S.; Mohapatra, S. K.; Graeve, O. A.; Misra, M. *Nanotechnology* **2008**, *19*, 445607−1−445607−1.
(19) Rather, S.; Mehraj-ud-din, N.; Zacharia, R.; Hwang, S. W.; Kim, A. R.; Nahm, K. S. *Int. J. Hydrogen Energy* **2009**, *34*, 961−966.
(20) Yang, A.; Tao, X.; Wang, R.; Lee, S.; Surya, C. *Appl. Phys. Lett.* **2007**, *91*, 133110−1−133110−3.
(21) Yang, M.; Kim, D.-H.; Kim, W.-S.; Kang, T. J.; Lee, B. Y.; Hong, S.; Kim, Y. H.; Hong, S.-H. *Nanotechnology* **2010**, *21*, 215501−1−215501−7.
(22) Wongchoosuk, C.; Wisitsoraat, A.; Phokkaratkul, D.; Tuantranont, A.; Kerdcharoen, T. *Sensors* **2010**, *10*, 7705−7715.
(23) Orel, B.; Groselj, N.; Krasovec, U. O.; Gabrscek, M.; Bukovec, P.; Reisfeld, R. *Sens. Actuators, B* **1998**, *50*, 234−245.
(24) Georg, A.; Graf, W.; Neumann, R.; Wittwer, V. *Solid State Ionics* **2000**, *127*, 319−328.
(25) Lim, S. H.; Luo, J.; Zhong, Z.; Ji, W.; Lin. *J. Inorg. Chem.* **2005**, *44*, 4124−4126.
(26) Bavykin, D. V.; Lapkin, A. A.; Plucinski, P. K.; Friedrich, J. M.; Walsh, F. C. *J. Phys. Chem. B* **2005**, *109*, 19422−19427.
(27) Silambarasan, D.; Surya, V. J.; Vasu, V.; Iyakutti, K. *Int. J. Hydrogen Energy* **2011**, *36*, 3574−3579.
(28) Wu, X. M.; Wang, Y.; Dong, K. M.; Zhou, J M.; Lin, G. D.; Zhang, H. B. *Acta. Chim. Sinica* **2005**, *63*, 484−490.
(29) Silambarasan, D.; Vasu, V.; Surya, V. J.; Iyakutti, K. *IEEE Trans. Nanotechnol.* **2012**, *11*, 1047−1053.
(30) Ansari, S. G.; Dar, M. A.; Dhage, M. S.; Kim, Y. S.; Ansari, Z. A.; Al-Hajry, A.; Shin, H.-S. *Rev. Sci. Instrum.* **2009**, *80*, 045112−1−045112−6.
(31) Boulova, M.; Rosman, N.; Bouvier, P.; Lucazeau, G. *J. Phys.: Condens. Matter* **2002**, *14*, 5849−5863.
(32) Regragui, M.; Addou, M.; Outzourhi, A.; Bernede, J. C.; Idrissi, E. E.; Benseddik, E.; Kachouane, A. *Thin Solid Films* **2000**, *358*, 40−45.
(33) Parker, J. C.; Siegel, R. W. *Appl. Phys. Lett.* **1990**, *57*, 943−945.
(34) Subrahmanyam, K. S.; Prashant, K.; Urmimala, M.; Govindaraj, A.; Hembram, K. P. S. S.; Waghmare, U. V.; Rao, C. N. R. *Proc. Natl. Acad. Sci. U.S.A.* **2011**, *108*, 2674−2677.
(35) Sankaran, M.; Viswanathan, B. *Ind. J. Chem.* **2008**, *47*, 808−814.
(36) Badzian, A.; Badzian, T.; Breval, E.; Piotrowski, A. *Thin Solid Films* **2001**, *398*−*399*, 170−174.
(37) Zhang, G.; Qi, P.; Wang, X.; Lu, Y.; Mann, D.; Li, H.; Dai, H. *J. Am. Chem. Soc.* **2006**, *128*, 6026−6027.
(38) Ioannatos, G. E.; Verykios, X. E. *Int. J. Hydrogen Energy* **2010**, *35*, 622−628.
(39) Durgun, E.; Ciraci, S.; Yildirim, T. *Phys. Rev. B* **2008**, *77*, 085405−1−085405−9.

(40) Lochan, R. C.; Head-Gordon, M. *Phys. Chem. Chem. Phys.* **2006**, *8*, 1357−1370.
(41) Li, Y. W.; Yang, F. H.; Yang, R. T. *J. Phys. Chem. C* **2007**, *111*, 3405−3411.
(42) Contescu, C. I.; Brown, C. M.; Liu, Y.; Bhat, V. V.; Gallego, N. C. *J. Phys. Chem. C* **2009**, *113*, 5886−5890.
(43) Campesi, R.; Cuevas, F.; Gadiou, R.; Leroy, E.; Hirscher, M.; Vix-Guterl, C.; Latroche, M. *Carbon* **2008**, *46*, 206−214.